JEE Journal of Ecological Engineering

Journal of Ecological Engineering 2024, 25(8), 54–61
https://doi.org/10.12911/22998993/189672
ISSN 2299–8993, License CC-BY 4.0

Received: 2024.05.18
Accepted: 2024.06.12
Published: 2024.07.01

Valorization of Tropical Almond (*Terminalia catappa*) Leaves into Iron-Containing Activated Carbon for Rapid Catalytic Degradation of Methylene Blue with Hydrogen Peroxide

Nhi Thi Kieu Nguyen[1,2], Duong Thi Thuy Le[1,2], Khang Dinh Vo[1,2], Linh Tung Huynh[1,2], Hung Minh Nguyen[1,2], Tuyet-Mai Tran-Thuy[1,2], Long Quang Nguyen[1,2], Dung Van Nguyen[1,2*]

[1] Faculty of Chemical Engineering, Ho Chi Minh City University of Technology (HCMUT), 268 Ly Thuong Kiet Street, District 10, Ho Chi Minh City, Vietnam

[2] Vietnam National University Ho Chi Minh City, Linh Trung Ward, Thu Duc City, Ho Chi Minh City, Vietnam

* Corresponding author's e-mail: nvdung@hcmut.edu.vn

ABSTRACT

This study sought to use tropical almond leaves (TALs) for the simple fabrication of iron-containing activated carbon (IAC). Iron precursor ($FeCl_3$) and activating agent (KOH) were sequentially preloaded in TALs. One-pot pyrolysis then generated iron-based particles (8.7 wt%), mainly metallic iron crystals, within AC support. The specific saturation magnetization of IAC was measured to be 48.9 emu/g, highlighting its ability to be efficiently separated using external magnetic fields. Moreover, the activation process yielded IAC with a large total volume of 0.28 cm^3/g and a high specific surface area of 463 m^2/g. Accordingly, IAC was investigated as an oxidation catalyst to degrade methylene blue (MB) by H_2O_2. At pH 3.0, 800 ppm H_2O_2, and 0.10 g/L IAC, 95.3% of MB (200 ppm) was removed after 30 min of adsorption and 60 min of oxidation. Altogether, iron-containing activated carbon from fallen leaves of tropical almonds proved its potential for robust methylene blue degradation by H_2O_2.

Keywords: zero-valent iron, activated carbon, tropical almond leaves, one-pot strategy, Fenton-like process, methylene blue.

INTRODUCTION

Tropical almond (*Terminalia catappa*) is a sizable tree that is widely found in tropical and subtropical areas [1]. The tree is considered decorative as its enormous leaves offer extensive shade [2]. During the dry season, TALs undergo a color change, turning pinkish-reddish or yellow-brown before eventually dropping to the ground [3, 4]. Although TALs can be used to create herbal medicines [5, 6], this demand is very limited. Indeed, a substantial volume of fallen leaves is normally left for natural decomposition or gathered as urban waste. Thus, TALs are an abundant and underutilized biomass resource. Due to their large size, TALs can be collected with less effort than other small leaves. Their soft structure might also be advantageous for further processes.

Currently, water contamination caused by organic compounds originating from diverse manufacturing processes is a notable ecological issue [7]. Wastewater commonly contains organic contaminants such as pesticides, medicines, detergents, solvents, and colorants [8, 9]. These chemicals persist in the environment, leading to bioaccumulation in the food chain and detrimental impacts on aquatic organisms [10, 11]. They also pose possible concerns for human health through contaminated water sources [12]. In order to mitigate these impacts, it is necessary to properly treat organic pollutants before releasing them into water bodies. Nevertheless, conventional treatment methods have such limitations,

especially for recalcitrant organic contaminants [13, 14]. Thus, it necessitates the development of advanced treatment techniques. Fenton and Fenton-like advanced oxidation processes are a promising solution for the treatment of organic pollutants in wastewater [15, 16]. These processes convert hydrogen peroxide (H_2O_2) into highly reactive hydroxyl radicals (•OH), which can degrade a wide variety of organic contaminants into less harmful substances like water and carbon dioxide [17]. For that purpose, the classical Fenton process employs ferrous ions (Fe^{2+}), while Fenton-like processes extend the utilization of ferric ions (Fe^{3+}) or other transition metal ions [18]. Although these homogeneous processes are simple and effective, the handling and disposal of solid sludge pose challenges [19]. Therefore, heterogeneous Fenton-like processes using solid catalysts are more favorable. In recent years, metallic iron (Fe(0)) has been increasingly explored as a potential heterogeneous catalyst due to its high reactivity, low cost, and environmental friendliness [20, 21]. Indeed, Fe(0) particles can continuously provide Fe(II) to produce hydroxyl radicals from H_2O_2 [22]. However, Fe(0) particles are easily agglomerated, causing a decline in their catalytic performance during use [23, 24]. To overcome this shortcoming, Fe(0) particles could be immobilized on proper supports.

Activated carbon (AC) is widely recognized as a highly effective support for Fe(0) particles, offering numerous advantages such as a highly porous structure, excellent adsorption properties, chemical stability, cost-effectiveness, and eco-friendliness [25, 26]. These properties improve the catalytic activity, stability, and reusability of Fe(0) catalysts [27]. To immobilize Fe(0) particles in AC, different methods have been developed. In previous studies, direct $FeCl_3$ activation of biomass mainly forms Fe_3O_4 crystals within biochar base [28, 29]. To obtain Fe(0) and AC simultaneously, an improved procedure was introduced recently [30]. Biomass is loaded consecutively with an iron precursor ($FeCl_3$) and KOH. One-pot pyrolysis can then form IAC. In addition to the properties mentioned before, the new composite possesses magnetic properties for convenient separation. Because of these advantages, the current study applied the procedure to fabricate IAC from TALs. The catalytic activity of IAC was explored for methylene blue degradation with H_2O_2.

MATERIALS AND METHODS

Materials

Fallen leaves of tropical almonds were gathered at Ly Thuong Kiet campus, HCMUT, Ho Chi Minh City, Vietnam. After being cleaned with tap water and distilled water, the leaves were dried at 110 °C for 24 h. The raw material was pulverized into a fine powder and stored in a jar for later use.

Fabrication of iron-containing activated carbon from tropical almond leaves

First, 4.00 g of TAL powder, 1.333 g of $FeCl_3.6H_2O$, and 50.0 mL of distilled water were put together in a 250 mL beaker. After agitating for 2 h at room temperature, 50.0 mL of an aqueous solution containing 12.00 g of KOH was poured into the beaker. Another 2 h of continuous mixing was kept before the sample was dried for 24 h at 110 °C. The dried material was pulverized into a fine powder before being placed in a tube furnace with a heating rate of 5 °C/min. The pyrolysis was then carried out at 600 °C for 1 h under a nitrogen atmosphere. Lastly, the pyrolyzed product was rinsed carefully and evaporated to obtain IAC. For comparison, AC was prepared using the same procedure but without $FeCl_3.6H_2O$.

Characterization of iron-containing activated carbon

The crystalline structure of IAC was studied by X-ray diffraction (XRD) using a Bruker AXS D8 diffractometer. The 2θ range was 10–80°, and Cu-Kα radiation (λ = 1.5418 Å) was used as the target. Scanning electron microscopy (SEM) images were recorded with a JEOL JSM-IT200 instrument. Functional groups present on the surface of IAC were explored by Fourier transform infrared (FTIR) spectroscopy using a Bruker VERTEX 70 spectrometer. Nitrogen adsorption and desorption isotherms of IAC were measured at 77 K on a Micromeritics Tristar II Plus instrument. The sample was outgassed at 150 °C for 12 h. The BJH method was used to express pore size distribution. Specific surface area was calculated by the BET equation. Total pore volume was obtained at P/P_o = 0.997. Micropore and mesopore volumes were estimated using the t-plot method. A PerkinElmer Optima 7300 DV ICP-OES instrument was used for the compositional analysis

of IAC. Iron was extracted from IAC using concentrated HNO_3 at 50 °C for 1 h. The magnetic measurement of IAC was examined using a VSM at room temperature.

Degradation of methylene blue using iron-containing activated carbon

Catalytic degradation of MB was performed in 250-mL flasks at room temperature (30 °C). In a typical experiment, a specific IAC dosage was added to 100 mL of MB solution (200 ppm). Initial pH values were altered with NaOH (0.10 M) and HCl (0.10 M) solutions. The mixture underwent continual stirring throughout the treatment. After the adsorption step took 30 min, H_2O_2 (800 ppm) was promptly added to the suspension to commence the oxidation step. At specified times, each 1.00 mL of suspension was withdrawn from flasks and added to 9.00 mL of an aqueous solution containing $Na_2S_2O_3$ (2.00 g/L) and phosphate buffer. IAC was separated from treated mixtures and MB concentrations were analyzed using a spectrophotometer at 664 nm. The MB adsorption capacity and total MB removal were computed as follows:

$$\text{MB adsorption capacity (mg/g)} = \frac{200 - C_0}{C_A} \quad (1)$$

$$\text{Total MB removal (\%)} = \frac{200 - C_{60}}{200} \times 100\% \quad (2)$$

where: C_A (g/L) was AC or IAC dosages, while the initial MB concentration was 200 ppm. C_0 and C_{60} (ppm) were MB concentrations after 30 min of adsorption and after 60 min of oxidation, respectively.

RESULTS AND DISCUSSION

Properties of iron-containing activated carbon

Figure 1 illustrates the XRD pattern of IAC. Distinct peaks were observed at $2\theta = 44.6$ and 65.0° oriented along the (110) and (200) planes of metallic iron crystals (ICDD 00-001-1262). In contrast, other peaks lacked sufficient clarity to discern certain crystals. Hence, iron loaded in AC predominantly existed in the form of Fe(0) crystals. Their formation pathway is proposed as follows:

$$FeCl_3 + 3KOH \rightarrow Fe(OH)_3 + 3KCl \quad (3)$$

$$TAL \rightarrow C, CO, H_2, H_2O \quad (4)$$

$$Fe(OH)_3 \rightarrow Fe_2O_3 + C, CO, H_2 \rightarrow Fe_3O_4 + C, CO, H_2 \rightarrow Fe(0) \quad (5)$$

As previously presented, $FeCl_3$ was initially impregnated into TAL powder. This process could disperse Fe^{3+} ions within vacant spaces of TAL biomass. Subsequently, the addition of KOH could generate $Fe(OH)_3$ precipitate in TAL structure. During pyrolysis, the biomass could be carbonized and emit such gas-phase compounds, while $Fe(OH)_3$ was dehydrated. Consecutive reactions have the potential to convert Fe_2O_3 into Fe(0). At 600 °C, excess KOH could also activate the carbon framework. As a result, carbonization, reduction, and activation could occur simultaneously, leading to the generation of Fe(0) particles within AC support. This innovative approach differs from previous methodologies, which commonly involve multiple steps and costly reducing agents like $NaBH_4$.

The nitrogen adsorption and desorption isotherms of IAC are presented in Figure 2. The dramatic increase in the adsorbed volume when P/P_o grew from 0.0004 to 0.05 revealed the existence of micropores in IAC. Next, the hysteresis loop in P/P_o range from 0.38 to 0.99 affirmed capillary condensation in mesopores. In detail, BJH pore size distribution demonstrated that IAC developed a hierarchically microporous and mesoporous structure with a typical mesopore size of 4.1 nm. Furthermore, total pore volume of IAC was 0.28 cm^3/g, including 50% of micropore volume (0.14 cm^3/g) and 50% of mesopore volume (0.14 cm^3/g). The hierarchically porous structure might improve mass transfer, while a high specific

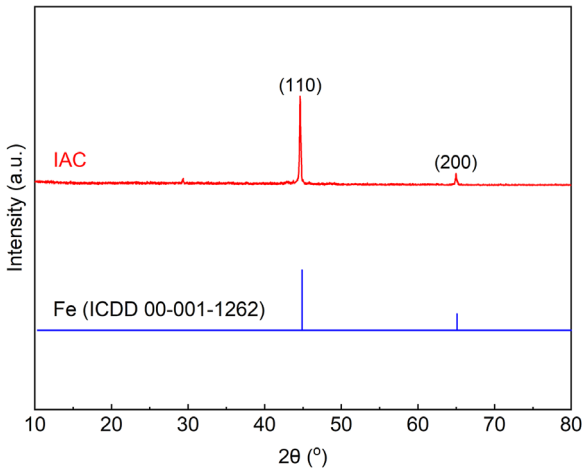

Figure 1. XRD pattern of IAC

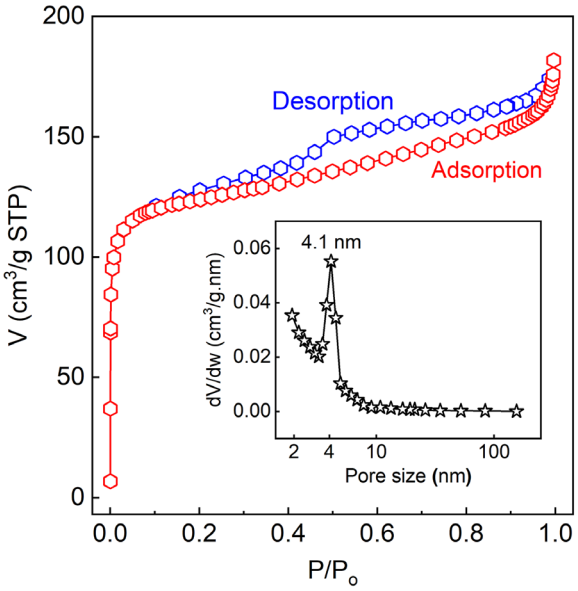

Figure 2. Nitrogen adsorption and desorption isotherms of IAC

surface area of 463 m^2/g might enhance surface interaction during IAC use. Figure 3 shows the FTIR spectroscopy of IAC. The stretching vibration of O–H bonding could be determined at 3436 cm^{-1}, while the vibrating peaks at 1436 and 874 cm^{-1} are predicted to belong to C–H bonding. Moreover, the vibrating bands at 1617 cm^{-1} could be present for C=C bonding and a peak of 1024 cm^{-1} affirmed the existence of C–O bonding. Hence, the pyrolysis condition still kept some polar functional groups on the IAC surface. Their existence could potentially strengthen the interaction of IAC with organic contaminants and oxidizing agents.

Figure 4 illustrates that IAC consisted of small fragments with various shapes and sizes, possibly as a result of the fine grinding process. In each fragment, such empty spaces with thin walls were observed. At the microscale, these cavities

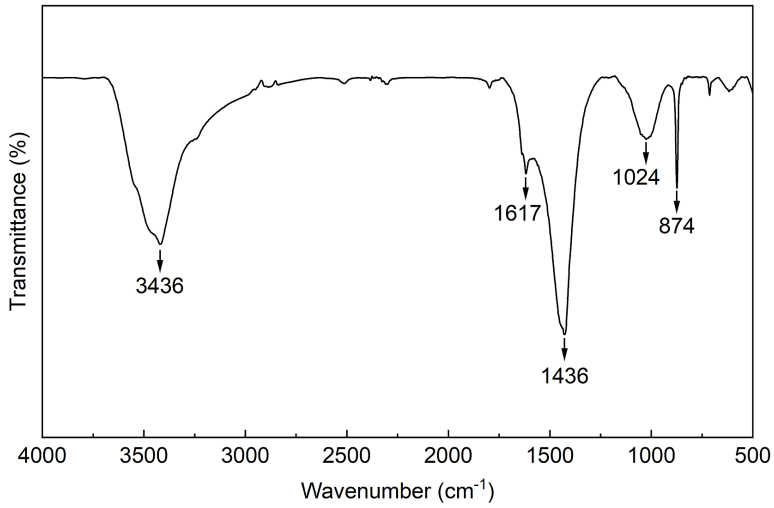

Figure 3. FTIR spectroscopy of IAC

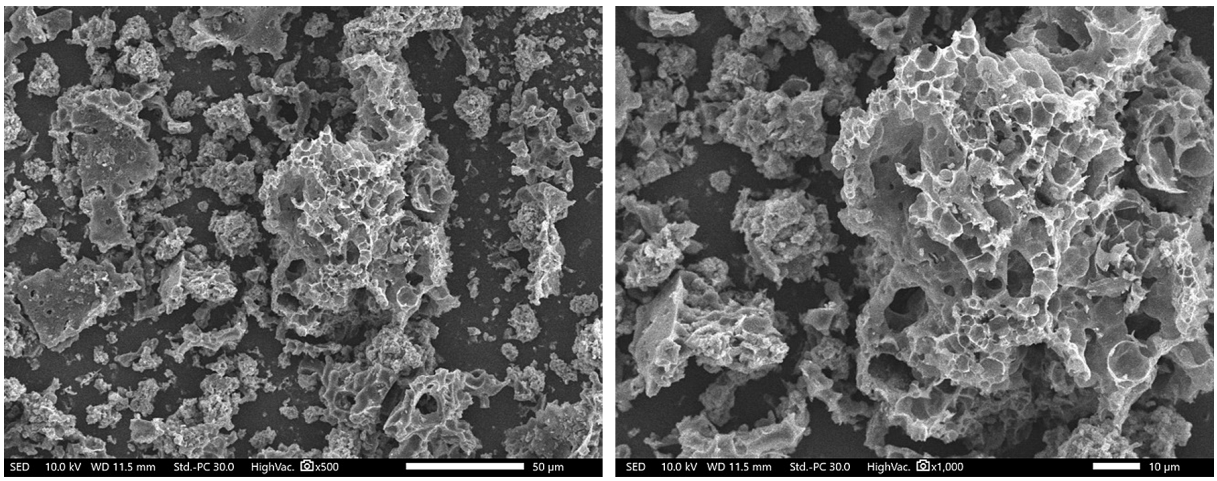

Figure 4. SEM images of IAC

may originate from the natural structure of TALs rather than being formed through activation. In general, the spacious cavities might be advantageous for surface interaction during IAC use.

The magnetic properties of IAC were studied with VSM (Figure 5). The narrow hysteresis found indicates that IAC was susceptible to magnetization and demagnetization by the alteration of external magnetic fields. Furthermore, the specific saturation magnetization of IAC reached 48.9 emu/g, whereas iron only accounted for 8.7 wt% of IAC. This result could be derived from the powerful magnetic properties of Fe(0) particles in IAC. The composite is therefore capable of magnetic separation and recovery.

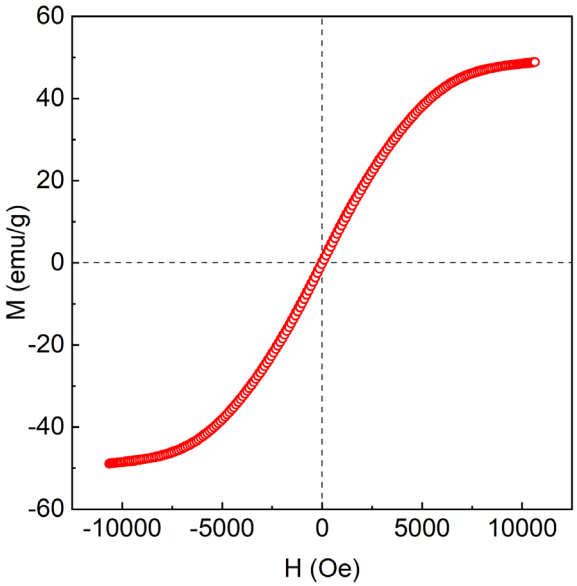

Figure 5. VSM curve of IAC

Degradation of methylene blue using iron-containing activated carbon

MB can be removed by IAC through not only oxidation but also adsorption pathways. Hence, adsorption was carried out in the first 30 min, and then H_2O_2 was added for further oxidation. In general, MB concentration slightly declined and almost reached equilibrium after 30 min of adsorption. At pH 3.0, the MB adsorption capacities of IAC and AC were 55 and 140 mg/g, respectively. Accordingly, only 2.8–7.0% of MB was removed in the first step, which was suitable for the evaluation of the next catalytic oxidation step.

Figure 6 shows that H_2O_2 alone (no catalyst) was almost incapable of directly degrading MB during 60 min. To improve MB degradation, an appropriate catalyst must be used. In the case of AC, MB concentration generally remained in the oxidation step. On the contrary, the presence of IAC provided rapid MB elimination. The comparison revealed that AC served as a support, while Fe(0) particles acted as catalytic sites for MB degradation. According to the Fenton-like process, organic pollutants can be oxidized by reactive ·OH radicals [31]. The existence of Fe(0) particles in IAC could enhance the production of ·OH radicals from H_2O_2 as follows:

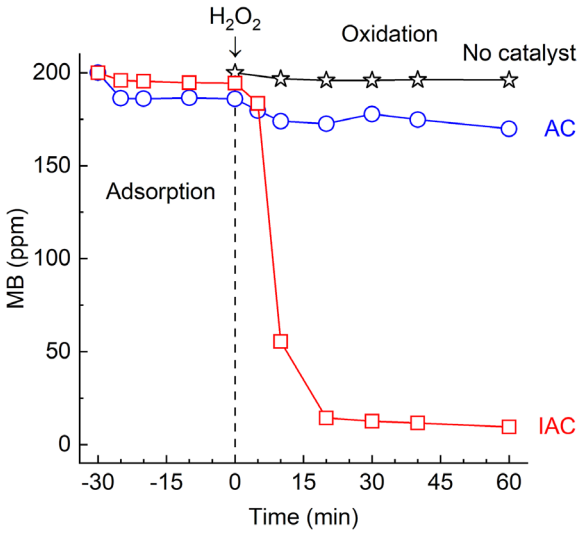

Figure 6. MB degradation with H_2O_2 catalyzed by AC and IAC (0.10 g/L catalyst, pH 3.0, 800 ppm H_2O_2)

$$Fe(0) + H_2O_2 + 2H^+ \rightarrow Fe(II) + 2H_2O \quad (6)$$

$$Fe(II) + H_2O_2 \rightarrow Fe(III) + \bullet OH + OH^- \quad (7)$$

$$Fe(III) + H_2O_2 \rightarrow Fe(II) + H^+ + \bullet OOH \quad (8)$$

$$Fe(0) + 2Fe(III) \rightarrow 3Fe(II) \quad (9)$$

$$\bullet OH + MB \rightarrow Intermediates \rightarrow CO_2 + H_2O \quad (10)$$

Under acidic media, Fe(0) could be corroded into Fe(II) [32]. Fe(II) could then form ·OH radicals from H_2O_2. Notably, Fe(II) could be regenerated from Fe(III) via Equation 8. Furthermore, Fe(0) is capable of rapidly reducing Fe(III) to Fe(II) [33, 34]. As a result, Fe(0) is served as the source of Fe(II).

The effect of IAC dosage on MB degradation is illustrated in Figure 7. As previously presented, H_2O_2 without IAC could not directly eliminate MB during 60 min. As IAC was employed, MB degradation was accelerated drastically. In addition, the degradation rate improved gradually when IAC dosage rose from 0.05 to 0.20 g/L.

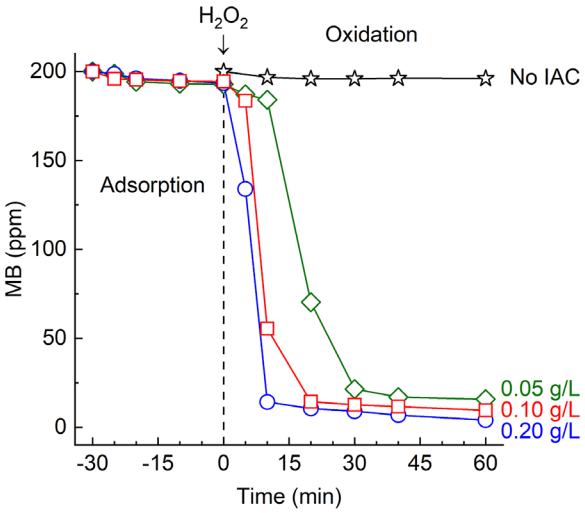

Figure 7. Effect of IAC dosage on MB degradation with H_2O_2 (pH 3.0, 800 ppm H_2O_2)

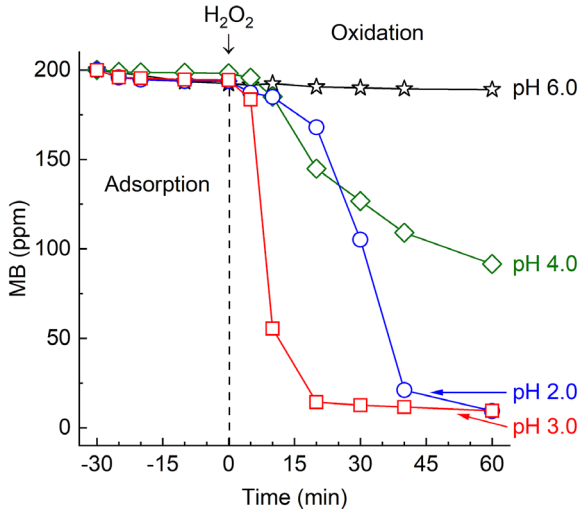

Figure 8. Effect of pH on MB degradation with H_2O_2 catalyzed by IAC (0.10 g/L IAC, 800 ppm H_2O_2)

A higher IAC dosage could provide more active sites, thereby accelerating the production of ·OH radicals. However, too much IAC dosage might cause wasting and negative effects. In detail, excessive Fe(II) might consume ●OH radicals [35, 36], as follows:

$$Fe(II) + \bullet OH \rightarrow Fe(III) + OH^- \quad (11)$$

Figure 8 demonstrates that pH significantly influenced MB degradation, with the highest rate occurring at pH 3.0. High proton concentration at low pH could accelerate the corrosion of Fe(0) into Fe(II), thereby significantly improving the rate of MB degradation [20]. Nonetheless, MB degradation at pH 2.0 was weaker than that at pH 3.0. Very low pH greatly enhanced the loss of ·OH by the scavenging effect [18, 37]:

$$\bullet OH + H^+ + e^- \rightarrow H_2O \quad (12)$$

On the contrary, as pH increased from 3.0 to 4.0, total MB removal decreased remarkably from 95.3% to 54.3%. Even MB degradation became negligible at pH 6.0. The decrease in the oxidation potential of ●OH could be attributed to the decline in MB degradation at higher pH values [18, 20]. In addition, higher pH values may promote H_2O_2 decomposition into O_2 rather than ●OH [22, 37]. Notably, the corrosion of Fe(0) into Fe(II) could be weakened at high pH. Fe(II) and Fe(III) ions may create precipitates located on IAC surface, resulting in further corrosion prevention [31]. Thus, pH 3.0 was favorable for IAC catalyst, similar to previous studies for the Fenton-like reaction catalyzed by metallic iron [18].

CONCLUSION

Fallen leaves of tropical almonds are regarded as municipal waste with limited use. TALs were therefore valorized for the simple fabrication of iron-containing activated carbon using $FeCl_3$ as an iron precursor and KOH as an activating agent. As a result, metallic iron crystals were identified as the primary iron-based ones. With 8.7 wt% of iron introduced into IAC, its specific saturation magnetization was enhanced to 48.9 emu/g, providing robust support for magnetic separation. In addition, the activation process yielded IAC with a total volume of 0.28 cm^3/g and a specific surface area of 463 m^2/g. Accordingly, IAC was explored for catalytic MB degradation by H_2O_2. In the first 30-min adsorption, 0.10 g/L of IAC at pH 3.0 slightly eliminated 2.8% of MB (200 ppm) with an adsorption capacity of 55 mg/g. As 800 ppm H_2O_2 was added, a total of 95.3% of MB was treated after 60 min of oxidation. Overall, iron-containing activated carbon prepared from tropical almond leaves is favorable for the expeditious Fenton-like degradation of methylene blue.

Acknowledgments

This research is funded by Vietnam National University HoChiMinh City (VNU-HCM) under grant number: 562-2023-20-04. We acknowledge Ho Chi Minh City University of Technology (HCMUT), VNU-HCM for supporting this study.

REFERENCES

1. Ko T.-F., Weng Y.-M., Lin S.-B. and Chiou R.Y.Y. 2003. Antimutagenicity of supercritical CO_2 extracts of *Terminalia catappa* leaves and cytotoxicity of the extracts to human hepatoma cells. Journal of Agricultural and Food Chemistry, 51(12), 3564–3567.
2. Vinturelle R., Cabral T.d.S., Oliveira P.C.O. d., Salles J.P., Faria J.V., Teixeira G.P., Faria R.X., Veloso M.C.C., Romeiro G.A. and Chagas E.F. d. 2024. Slow pyrolysis of *Terminalia catappa* L. municipal solid waste and the use of the aqueous fraction produced for bovine mastitis control. Biochemistry and Biophysics Reports, 38, 101704.
3. Pereira H., Simões R. and Miranda I. 2023. Cuticular waxes and cutin in *Terminalia catappa* leaves from the Equatorial São Tomé and Príncipe islands. Molecules, 28(17), 6365.
4. Eddy N.O., Ekwumemgbo P.A. and Mamza P.A.P. 2009. Ethanol extract of *Terminalia catappa* as a green inhibitor for the corrosion of mild steel in H_2SO_4. Green Chemistry Letters and Reviews, 2(4), 223–231.
5. Oyeleye S.I., Adebayo A.A., Ogunsuyi O.B., Dada F.A. and Oboh G. 2017. Phenolic profile and enzyme inhibitory activities of almond (*Terminalia catappa*) leaf and stem bark. International Journal of Food Properties, 20(3), 2810–2821.
6. Madhavan K., Rukayadi Y. and Abdul-Mutalib N.A. 2023. Controlling vegetative cells and spores growth of *Bacillus* spp. using ethanolic *Ketapang* (*Terminalia catappa* L.) leaf extract. Heliyon, 9(8), e18749.
7. Sousa J.C.G., Ribeiro A.R., Barbosa M.O., Pereira M.F.R. and Silva A.M.T. 2018. A review on environmental monitoring of water organic pollutants identified by EU guidelines. Journal of Hazardous Materials, 344, 146–162.
8. Lu F. and Astruc D. 2020. Nanocatalysts and other nanomaterials for water remediation from organic pollutants. Coordination Chemistry Reviews, 408, 213180.
9. Chen J.-Q., Sharifzadeh Z., Bigdeli F., Gholizadeh S., Li Z., Hu M.-L. and Morsali A. 2023. MOF composites as high potential materials for hazardous organic contaminants removal in aqueous environments. Journal of Environmental Chemical Engineering, 11(2), 109469.
10. Rasheed T., Shafi S., Bilal M., Hussain T., Sher F. and Rizwan K. 2020. Surfactants-based remediation as an effective approach for removal of environmental pollutants–A review. Journal of Molecular Liquids, 318, 113960.
11. Titchou F.E., Zazou H., Afanga H., El Gaayda J., Ait Akbour R., Nidheesh P.V. and Hamdani M. 2021. Removal of organic pollutants from wastewater by advanced oxidation processes and its combination with membrane processes. Chemical Engineering and Processing - Process Intensification, 169, 108631.
12. Mukhopadhyay A., Duttagupta S. and Mukherjee A. 2022. Emerging organic contaminants in global community drinking water sources and supply: A review of occurrence, processes and remediation. Journal of Environmental Chemical Engineering, 10(3), 107560.
13. Morin-Crini N., Lichtfouse E., Fourmentin M., Ribeiro A.R.L., Noutsopoulos C., Mapelli F., Fenyvesi É., Vieira M.G.A., Picos-Corrales L.A., Moreno-Piraján J.C., Giraldo L., Sohajda T., Huq M.M., Soltan J., Torri G., Magureanu M., Bradu C. and Crini G. 2022. Removal of emerging contaminants from wastewater using advanced treatments. A review. Environmental Chemistry Letters, 20(2), 1333–1375.
14. Aravind kumar J., Krithiga T., Sathish S., Renita A.A., Prabu D., Lokesh S., Geetha R., Namasivayam S.K.R. and Sillanpaa M. 2022. Persistent organic pollutants in water resources: Fate, occurrence, characterization and risk analysis. Science of The Total Environment, 831, 154808.
15. Liu Y. and Wang J. 2023. Multivalent metal catalysts in Fenton/Fenton-like oxidation system: A critical review. Chemical Engineering Journal, 466, 143147.
16. Nasir M.J., Kadhum Z.F., Kariem N.O. and Jasim Z.M. 2022. Removal of sesame oil from artificial wastewater applying fenton process and comparing it with actual wastewater. Journal of Ecological Engineering, 23(10), 248–254.
17. Shokri A. and Fard M.S. 2022. A critical review in Fenton-like approach for the removal of pollutants in the aqueous environment. Environmental Challenges, 7, 100534.
18. Wang N., Zheng T., Zhang G. and Wang P. 2016. A review on Fenton-like processes for organic wastewater treatment. Journal of Environmental Chemical Engineering, 4(1), 762–787.
19. Hussain S., Aneggi E. and Goi D. 2021. Catalytic activity of metals in heterogeneous Fenton-like oxidation of wastewater contaminants: a review. Environmental Chemistry Letters, 19(3), 2405–2424.
20. Liang L., Cheng L., Zhang Y., Wang Q., Wu Q., Xue Y. and Meng X. 2020. Efficiency and mechanisms of rhodamine B degradation in Fenton-like systems based on zero-valent iron. RSC Advances, 10(48), 28509–28515.
21. Conde-Cid M., Paíga P., Moreira M.M., Albergaria J.T., Álvarez-Rodríguez E., Arias-Estévez M. and Delerue-Matos C. 2021. Sulfadiazine removal using green zero-valent iron nanoparticles: A low-cost and eco-friendly alternative technology for water remediation. Environmental Research, 198, 110451.
22. Zha S., Cheng Y., Gao Y., Chen Z., Megharaj M. and Naidu R. 2014. Nanoscale zero-valent iron as a catalyst for heterogeneous Fenton oxidation of amoxicillin. Chemical Engineering Journal, 255, 141–148.

23. Xie S., Su J., Zhao J., Yang H. and Qian H. 2022. An amorphous zero-valent iron decorated by Fe_3O_4 significantly improves the Fenton-like reaction. Journal of Alloys and Compounds, 929, 167306.
24. Xia J., Shen Y., Zhang H., Hu X., Mian M. M. and Zhang W.-H. 2022. Synthesis of magnetic nZVI@ biochar catalyst from acid precipitated black liquor and Fenton sludge and its application for Fenton-like removal of rhodamine B dye. Industrial Crops and Products, 187, 115449.
25. Tseng H.-H., Su J.-G. and Liang C. 2011. Synthesis of granular activated carbon/zero valent iron composites for simultaneous adsorption/dechlorination of trichloroethylene. Journal of Hazardous Materials, 192(2), 500–506.
26. Messele S.A., Soares O.S.G.P., Órfão J.J.M., Bengoa C., Stüber F., Fortuny A., Fabregat A. and Font J. 2015. Effect of activated carbon surface chemistry on the activity of ZVI/AC catalysts for Fenton-like oxidation of phenol. Catalysis Today, 240, 73–79.
27. Messele S.A., Bengoa C., Stüber F., Fortuny A., Fabregat A. and Font J. 2016. Catalytic wet peroxide oxidation of phenol using nanoscale zero-valent iron supported on activated carbon. Desalination and Water Treatment, 57(11), 5155–5164.
28. Do T.V.T., Bui Q.L.N., Nguyen H.M., Lam H.H., Tran-Thuy T.-M., Nguyen L.Q., Ngo D.T.H. and Nguyen D.V. 2022. One-pot fabrication of magnetic biochar by $FeCl_3$-activation of lotus seedpod and its catalytic activity towards degradation of Orange G. Mater. Res. Express, 9, 105601.
29. Nguyen H.M., Truong T.B., Nguyen H.-H.T., Tran P.T., Tran-Thuy T.-M., Nguyen L.Q. and Nguyen D.V. 2023. Catalytic ozonation of Ponceau 4R using multifunctional magnetic biochar prepared from rubber seed shell. Journal of Ecological Engineering, 24(12), 143–151.
30. Nguyen H.M., Tran A.T., Nguyen D.N.L., Lam H.H., Tran-Thuy T.-M., Nguyen L.Q., Le T.X. and Nguyen D.V. 2023. One-pot fabrication of zero-valent iron-embedded activated carbon from rosemary distillation residues for malachite green removal. Mater. Res. Express, 10(8), 085603.
31. Rezaei F. and Vione D. 2018. Effect of pH on zero valent iron performance in heterogeneous Fenton and Fenton-like processes: A review. Molecules, 23(12), 3127.
32. Xu L. and Wang J. 2011. A heterogeneous Fenton-like system with nanoparticulate zero-valent iron for removal of 4-chloro-3-methyl phenol. Journal of Hazardous Materials, 186(1), 256–264.
33. Wang L., Yang J., Li Y., Lv J. and Zou J. 2016. Removal of chlorpheniramine in a nanoscale zero-valent iron induced heterogeneous Fenton system: Influencing factors and degradation intermediates. Chemical Engineering Journal, 284, 1058–1067.
34. Huang T., Zhang G., Zhang N., Ye J. and Lu P. 2018. Fe^0-H_2O_2 for advanced treatment of citric acid wastewater: Detailed study of catalyst after several times use. Chemical Engineering Journal, 336, 233–240.
35. Segura Y., Martínez F. and Melero J.A. 2013. Effective pharmaceutical wastewater degradation by Fenton oxidation with zero-valent iron. Applied Catalysis B: Environmental, 136–137, 64–69.
36. Zhang M.-h., Dong H., Zhao L., Wang D.-x. and Meng D. 2019. A review on Fenton process for organic wastewater treatment based on optimization perspective. Science of The Total Environment, 670, 110–121.
37. Lv X., Ma Y., Li Y. and Yang Q. 2020. Heterogeneous Fenton-like catalytic degradation of 2,4-dichlorophenoxyacetic acid by nano-scale zero-valent iron assembled on magnetite nanoparticles. Water, 12(10), 2909.